PCCP

Coupled *ab initio* potential energy surfaces for the reaction $Cl(^2P) + HCl \rightarrow ClH + Cl(^2P)$

Abigail J. Dobbyn,[a] J. N. L. Connor,*[a] Nicholas A. Besley,[b]† Peter J. Knowles[b] and George C. Schatz[c]‡

[a] *Department of Chemistry, University of Manchester, Manchester, UK M13 9PL*
[b] *School of Chemistry, University of Birmingham, Edgbaston, Birmingham, UK B15 2TT*
[c] *Theoretical Chemistry Group, Chemistry Division, Argonne National Laboratory, IL 60439, USA*

Received 21st October 1998, Accepted 26th November 1998

We have constructed the $1\,^2A'$, $2\,^2A'$ and $1\,^2A''$ potential energy surfaces for the $Cl(^2P) + HCl \rightarrow ClH + Cl(^2P)$ reaction, together with the non-adiabatic coupling surface between the $1\,^2A'$ and $2\,^2A'$ states. All our calculations used the MOLPRO quantum chemistry package, with Dunning's correlation consistent augmented valence triple zeta 1-electron basis set. The $1\,^2A'$ and $1\,^2A''$ energies are calculated at the restricted open shell coupled cluster singles doubles with perturbative triples (RCCSD-T) level, whilst the $2\,^2A'$–$1\,^2A'$ energy difference and the non-adiabatic coupling are calculated *via* the multireference configuration interaction (MRCI) technique. The non-adiabatic coupling is evaluated from transition matrix elements of the angular momentum operator, namely $\langle 1\,^2A''|\hat{L}_x|1\,^2A'\rangle$ and $\langle 1\,^2A''|\hat{L}_x|2\,^2A'\rangle$. The surfaces in a diabatic representation are fitted to rotated-Morse cubic-spline functions. The empirical long-range potentials of Dubernet and Hutson (*J. Phys. Chem.*, 1994, **98**, 5844), together with empirical short range potentials, are then combined with the fitted *ab initio* surfaces to produce a set of global potential energy surfaces. Convergence tests show that the height of the barrier at C_{2v} geometries is 0.4361 eV for the $1\,^2B_1$ state, and occurs at a ClHCl bond angle of 137°. The collinear barrier heights are 0.4939 eV on the $^2\Sigma_u^+$ surface and 0.9416 eV on the $^2\Pi_g$ surface.

I Introduction

In recent years there has been much interest in the $Cl(^2P) + HCl \rightarrow ClH + Cl(^2P)$ reaction, which is an important prototype of a heavy + light-heavy atom reaction.[1] Although this reaction has often been studied within the Born–Oppenheimer (BO) approximation, *i.e.* assuming a single adiabatic potential energy surface (PES), there are actually three doublet PESs which correlate to the ground state of $Cl(^2P) + HCl$. For collinear geometries, in the $C_{\infty v}$ symmetry group, these are the singly degenerate $^2\Sigma^+$ state and the doubly degenerate $^2\Pi$ state. More generally, in the C_s symmetry group, the states are $1\,^2A'$, $2\,^2A'$ and $^2A''$ (where we write $^2A''$ rather than $1\,^2A''$ for simplicity of notation). On bending, the $^2\Sigma^+$ state correlates with one of A′ symmetry, whilst the $^2\Pi$ state splits into one state of A′ symmetry and another of A″. The naming conventions of the states in various symmetry groups are presented in Table 1.

At long-range the $^2\Pi$ potential surface lies lower in energy than the $^2\Sigma^+$ surface. This is because the singly occupied p orbital of the $^2\Pi$ state is perpendicular to the ClHCl molecular axis, so that the p orbital pointing towards the positively polarized H in HCl is doubly occupied, giving rise to a more favourable quadrupole–quadrupole interaction, than the converse ($^2\Sigma^+$) arrangement of the singly and doubly occupied p orbitals.[2] However, in the transition state region for the reaction, the $^2\Sigma^+$ surface lies lower in energy than the $^2\Pi$ surface. This is because there is a greater electrostatic repulsion between the doubly occupied p orbital lying along the molecular axis ($^2\Pi$) and HCl, than the case when the singly occupied p orbital lies along the molecular axis ($^2\Sigma^+$). Hence there is a crossing of the $^2\Sigma^+$ and $^2\Pi$ surface at some intermediate collinear geometry. For non-collinear geometries, this real crossing becomes avoided, producing a conical intersection between the $1\,^2A'$ and $2\,^2A'$ PESs.

It is clear that a complete description of the $Cl(^2P) + HCl$ reaction must go beyond the BO approximation and include all three PESs, as well as the non-adiabatic interaction between the $1\,^2A'$ and $2\,^2A'$ states. Indeed dynamical studies of this reaction are currently being carried out using coupled PESs.[3–5]

Many electronic-structure investigations have been made of the Cl + HCl system, although most of them consider only the ground adiabatic PES. An exception is the recent paper by

Table 1 Symmetries of the three electronic states correlating with the ground state of $Cl(^2P) + HCl$ in various symmetry groups[a]

C_s	C_{2v}	$C_{\infty v}$	$D_{\infty h}$
$1\,^2A'$	$1\,^2B_1$	$^2\Sigma^+$	$^2\Sigma_u^+$
$2\,^2A'$	$2\,^2B_1$	$^2\Pi$	$^2\Pi_g$
$^2A''$	$^2A_2$	$^2\Pi$	$^2\Pi_g$

[a] C_s corresponds to bent asymmetric geometries of ClHCl, C_{2v} to bent symmetric geometries of ClHCl, $C_{\infty v}$ to collinear asymmetric ClHCl, and $D_{\infty h}$ to collinear symmetric ClHCl. (The molecule is taken to be lying in the *xz* plane.)

† Present address: Department of Molecular Biology, The Scripps Research Institute, 10550 North Torrey Pines Road, La Jolla, CA 92037, USA.

‡ Visiting Scientist. Permanent address: Department of Chemistry, Northwestern University, Evanston, IL 60208-3113, USA.

Maierle *et al.*,[4] which incorporates the work of Dubernet and Hutson.[2] Many of these previous studies have focused on characterizing the transition state (TS).[6–11] Both *ab initio*[12–14] and semiempirical PESs,[15–17] such as the often used Bondi–Connor–Manz–Römelt (BCMR) extended London–Eyring–Polyani–Sato (LEPS) surface,[18] have been presented. Much of this earlier work has concentrated on the collinear configuration of the atoms with relatively few points computed for non-collinear geometries, despite the fact that the TS is significantly bent.[9]

The aim of this paper is to generate a set of globally valid *ab initio* PESs for the reaction $Cl(^2P) + HCl \rightarrow ClH + Cl(^2P)$, *i.e.* for the $1\,^2A'(\Psi_1^a, E_1)$, $2\,^2A'(\Psi_2^a, E_2)$ and $^2A''(\Psi_3^a, E_3)$ states, together with the non-adiabatic coupling PES between the $1\,^2A'$ and $2\,^2A'$ states. The adiabatic states $1\,^2A'(\Psi_1^a, E_1)$ and $2\,^2A'(\Psi_2^a, E_2)$ possess a mixture of 'Σ-like' and 'Π-like' character, especially near the avoided crossing between them. Our intention is to construct diabatic states (χ_{11}^d, H_{11}) and (χ_{22}^d, H_{22}) that are mainly of either 'Σ-like' or 'Π-like' character; the coupling diabatic potential $H_{12} \equiv H_{21}$ then describes the non-adiabatic coupling between the $1\,^2A'$ and $2\,^2A'$ states.

The structure of the paper is as follows. In Section II we give a detailed description of the *ab initio* methods used to evaluate the points on the PESs; the convergence tests for the 1-electron basis set are given in Section IIA. We describe in Section III the transformation from the adiabatic to the diabatic basis, together with some illustrative results. Section IV reports the geometries at which the calculations were carried out. The fitting of the computed *ab initio* points to rotated-Morse cubic-spline functions is presented in Section V, and the construction of a set of global PESs is outlined in Section VB. Some properties of the resulting surfaces are described in Section VI, and our conclusions are in Section VII.

II *Ab initio* electronic structure calculations

As discussed in the Introduction, a comprehensive understanding of the $Cl(^2P) + HCl$ reaction requires PESs for the $1\,^2A'$, $2\,^2A'$ and the $^2A''$ states, as well as for the non-adiabatic coupling between the $1\,^2A'$ and $2\,^2A'$ states. The quantum chemistry package MOLPRO[19] was used for all our calculations. In order to compute accurately these PESs, it is important to include a large proportion of the dynamic correlation energy. On the other hand, the static correlation energy should be less significant, since a single configuration state function is capable of describing the dissociation of the doublet ClHCl into closed-shell singlet HCl and the doublet Cl radical. Also it is desirable to use a method which is size extensive, given the relatively large number of electrons in our system.

One method which satisfies many of these criteria is the coupled cluster singles doubles (CCSD) technique;[20] for open-shell systems, we use the partially spin-adapted formalism (RCCSD).[21] To perform calculations to within 'chemical accuracy' ($\approx$0.05 eV) it is necessary to include contributions from connected triple excitations.[22] However, to do this exactly is computationally very expensive, and a more common and efficient method is to treat the triple excitations in a perturbative manner using the converged CCSD amplitudes. Of the several perturbative triples variants: CCSD[T],[23] CCSD(T)[24,25] and CCSD-T,[26] we have used the CCSD-T *ansatz*, which is correct to fourth order and includes important fifth order contributions.

Unfortunately, although the RCCSD-T approach is expected to work well for the evaluation of the $1\,^2A'$ and $^2A''$ PESs, it is not able to calculate the $2\,^2A'$ PES, nor to give any information about the non-adiabatic coupling between the $1\,^2A'$ and $2\,^2A'$ states, since single reference coupled cluster techniques are limited to the ground state of any given symmetry.

Methods which are able to evaluate excited state energies include multi-configurational self-consistent field (MCSCF),[27,28] second or third order complete active space perturbation theory (CASPT2/3),[29] and multi-reference configuration-interaction (MRCI).[30,31] We found in preliminary investigations of ClHCl that it is necessary to use the MRCI method to obtain the PESs in their correct energetic order, *i.e.* with the same wavefunction characteristics as the states calculated at the RCCSD-T level, *e.g.* 'Σ-like' or 'Π-like', and which also produces a non-adiabatic coupling which varies in a reasonably smooth manner with geometry. The active space we used for these MRCI calculations had five electrons in three orbitals correlating to the three p orbitals on Cl, *i.e.* the three-highest-energy occupied-orbitals, two of a′ symmetry and one of a″ symmetry. The energies of the $1\,^2A'$ and $2\,^2A'$ states were calculated together; the $^2A''$ energy was computed separately. In addition, the transition matrix elements $\langle ^2A''|\hat{L}_x|1\,^2A'\rangle$ and $\langle ^2A''|\hat{L}_x|2\,^2A'\rangle$, where $\hat{L}_x$ is the angular momentum operator along the x axis, were also evaluated, for use in the transformation to the diabatic basis (see Section IIIA).

The approach used to combine the RCCSD-T and MRCI results is presented in Section IIIB. It should be noted that MRCI is not size extensive; also using the relatively small active space described above is not expected to recover as much of the correlation energy as RCCSD-T. Thus it is believed that the $1\,^2A'$ and $^2A''$ energies are more accurate at the RCCSD-T level, though it is not thought that these relatively small deficiencies in the MRCI calculations will greatly affect the energy gap $2\,^2A'$–$1\,^2A'$ or the coupling potential.

We have outlined above one fundamental problem with the RCCSD-T method as applied to our system. We also experienced two further technical difficulties. *Firstly*, the RCCSD-T method requires a reference wavefunction, or a set of molecular orbitals (MOs). It is usual to use MOs produced by a restricted Hartree–Fock (RHF) calculation. However, at a large range of geometries the MOs obtained from RHF are symmetry broken, *i.e.* they are not symmetrical with respect to the two HCl bonds at C_{2v} geometries: we have solutions of the type Cl˙ H—Cl or Cl—H Cl˙ rather than (Cl—H—Cl)˙. This, no doubt, partly arises from the large amount of correlation energy in the system, and the fact that it is possible to *artificially* lower the energy of the system by localizing electrons on separate parts of it.

One way to obtain a set of symmetry clean orbitals, *i.e.* those that are correctly delocalized across the molecule, is to carry out a state-averaged (SA) MCSCF calculation. This calculation optimized the energies of six states, four of A′ symmetry and two of A″ symmetry. The active space involved the distribution of 11 electrons in four orbitals of a′ symmetry and two of a″ symmetry, *i.e.* the six highest-energy occupied-orbitals. Therefore each optimized orbital is associated with an optimized state, helping to ensure that the orbitals are physically reasonable. (The SCF orbitals from the $ClHCl^-$ ion were used as a starting point for these calculations.) Our intention was to use natural orbitals for the $1\,^2A'$ state in a RCCSD-T calculation of the $1\,^2A'$ state, and similarly natural orbitals for the $^2A''$ state for a RCCSD-T calculation of the $^2A''$ state.

This leads to our *second* technical difficulty which concerns, as hinted at earlier, the energetic ordering of the states when they possess a particular wavefunction character. For example, at collinearity the ordering of the $^2\Sigma^+$ and $^2\Pi$ states could be different in MCSCF (or indeed RHF) compared to RCCSD-T. This is because the position of the intersection seam between the $^2\Sigma^+$ and $^2\Pi$ states is very sensitive to the amount of correlation energy included in the calculations. In these cases, a RCCSD-T calculation starting with a reference wavefunction with the incorrect character did not converge to the correct energy. (It should be noted that a simple rotation of the two highest-energy occupied-orbitals by 90°, or the use

Table 2 Height (eV) and position of the barrier for the $^2\Sigma_u^+$ state of ClHCl, which is the ground state in $D_{\infty h}$, for different basis sets. The stationary point is characterized by a minimum in the symmetric stretching coordinate and a maximum in the antisymmetric stretching coordinate (and also the bending coordinate). The geometries are optimized at the RCCSD-T level

Basis	r_{HCl}/a_0	RCCSD	RCCSD[T]	RCCSD(T)	RCCSD-T
cc-pVDZ	2.815	0.6729	0.6018	0.6006	0.6015
cc-pVTZ	2.801	0.6459	0.5353	0.5350	0.5362
cc-pVQZ	2.799	0.6360	0.5126	0.5126	0.5138
cc-pV5Z	2.797	0.6332	0.5052	0.5053	0.5065
aug-cc-pVDZ	2.822	0.6292	0.5369	0.5365	0.5375
aug-cc-pVTZ − f(Cl)	2.802	0.6051	0.4828	0.4831	0.4845
aug-cc-pVTZ	2.801	0.6142	0.4922	0.4926	0.4939
aug-cc-pVQZ − g(Cl)	2.799	0.6181	0.4897	0.4900	0.4913
aug-cc-pVQZ	2.801[a]	0.6191	0.4904	0.4907	0.4920

[a] aug-cc-pVTZ geometry used.

of natural orbitals for the $2\,^2A'$ state did not result in a set of smooth energies as the CHCl bond angle varied.)

To overcome this problem it is necessary to use a reference wavefunction in the RCCSD-T method with the correct character. As noted above, the MRCI method can generally supply this.§ Thus we used the natural orbitals for the $1\,^2A'$ state from a MRCI calculation in a RCCSD-T evaluation of the energy of the $1\,^2A'$ state, and similarly for the $^2A''$ state. This use of natural orbitals is perhaps only possible due to the domination of the wavefunction by a single reference configuration, so that occupation of the virtual orbitals is always small.

We now summarize the procedure employed in the *ab initio* calculations of the PESs: 1. A SCF calculation on $ClHCl^-$, to generate an initial set of MOs. 2. A SA-MCSCF calculation, over six states, with eleven electrons in six active orbitals, to obtain symmetry clean MOs. 3. A second SA-MCSCF calculation to obtain one set of natural orbitals averaged over the three relevant states ($1\,^2A'$, $2\,^2A'$, $^2A''$) without any orbital optimization, using an active space of five electrons in three orbitals.¶ 4. A MRCI calculation for all three states, using the natural orbitals from step three and the same active space. Transition angular momentum matrix elements are also evaluated in this step. 5. A restricted open shell coupled cluster singles doubles with perturbative triples (RCCSD-T) calculation of the $1\,^2A'$ and $^2A''$ states using the natural orbitals from the MRCI calculation in step four. At collinear configurations, the energy of the $2\,^2A'$ state is also evaluated in a RCCSD-T calcuation, again using the corresponding MRCI natural orbitals. (This is possible since at collinearity the $1\,^2A'$ and $2\,^2A'$ states correlate to the $^2\Sigma^+$ and $^2\Pi$ states, and therefore have different symmetries.)

A Convergence tests

Before computing *ab initio* energies on a large grid of nuclear geometries, careful consideration must be given to the basis set. The choice of basis set involves a balance between accuracy and the CPU time required, keeping in mind the computational resources available. By performing calculations in which we progressively increase the size of the basis set, we can determine not only a suitable basis for the evaluation of the PESs, but we can also investigate PES properties which are critical to the dynamics, such as the height and position of transition states.

Our convergence tests did not employ the somewhat involved method described above (Section II). Instead the MOs were simply obtained at the RHF level, followed by RCCSD-T calculations. The justification for this is two-fold. Firstly, all the convergence tests were carried out in the symmetry groups $D_{\infty h}$ and C_{2v}, so that the MOs were forced to have the correct symmetry. Secondly, the calculations were done at geometries where the $1\,^2A'$ and $2\,^2A'$ states are well separated in energy, so their order is always correctly given by RHF. For each basis set the geometry of the symmetric linear, $D_{\infty h}$, and symmetric bent, C_{2v}, transition states were optimized, and convergence with respect to barrier heights checked. (A resolution of 1° was used in the ClHCl bond angle θ.)

We used Dunning's correlation consistent basis sets throughout.[32,33] The largest basis sets for which we report results are Dunning's cc-pV5Z and aug-cc-pVQZ. However, these basis sets would be impractical for the computation of a large grid of PES energies. We experimented with the removal of diffuse functions from the basis sets, but our final choice was aug-cc-pVTZ, which nearly reproduced the $^2\Sigma_u^+$ and $^2\Pi_g$ barrier heights from the aug-cc-pVQZ basis set (see Tables 2 and 3). [The aug-cc-pVTZ–f(Cl) basis set is identical to aug-cc-pVTZ except that the diffuse f atomic orbitals on Cl have been excluded. Similarly, the aug-cc-pVQZ–g(Cl) basis set is identical to aug-cc-pVQZ except that the diffuse g atomic orbitals on Cl have been excluded.] Similar, though not quite as good, levels of convergence for the aug-cc-pVTZ basis set were found for the C_{2v} transition state (see Table 4). In addition the variation of the dipole polarizability with basis set in Table 4 shows the importance of additional diffuse functions in the basis set, and also that there is little difference in the results from the aug-cc-pVTZ and aug-cc-pVQZ basis sets.

One important manifestation of orbital basis incompleteness is basis set superposition error (BSSE). Although in principle one ought to take account of BSSE, we have not done so, chiefly because it is not clear that BSSE can be unambiguously defined near the symmetrical transition state. However, it is possible to say that the effect of BSSE near the transition state is rather small compared to other sources of error; the standard counterpoise corrections[34] for HCl and Cl at the $^2\Sigma_u^+$ collinear saddle point with RCCSD-T/aug-cc-pVTZ are 0.015 and 0.043 eV respectively. Of course, BSSE will assume greater significance in the long-range, weak-interaction regions; however, in these regions BSSE is expected to be less important than other sources of error such as the neglect of spin–orbit coupling.

Discussion of convergence tests. The height of the collinear $^2\Pi_g$ barrier in Table 3 is significantly larger than the $^2\Sigma_u^+$ barrier height (Table 2). In our most accurate calculations (aug-cc-pVQZ and RCCSD-T) this difference is 0.4469 eV. Maierle *et al.*[4] found, using scaled PESs with a difference of 0.262 eV in the $^2\Sigma^+/^2\Pi$ barrier heights, that the $^2\Pi$ state had

§ We found in our evaluation of *ab initio* energies for the PESs that at one collinear geometry, very close to the intersection seam ($\phi = 35°$, $l = 1.80$ Å, where ϕ and l are defined in Section IV), the ordering of the states at the MRCI level is reversed from the ordering of the states at the RCCSD-T level.

¶ This step was only necessary for technical reasons because of the way MOLPRO calculates natural orbitals.

Table 3 Height (eV) and position of the barrier for the $^2\Pi_g$ state of ClHCl, which is the first excited state in $D_{\infty h}$, for different basis sets. The stationary point is characterized by a minimum in the symmetric stretching coordinate (and also the bending coordinate) and a maximum in the antisymmetric stretching coordinate. The geometries are optimized at the RCCSD-T level

Basis	r_{HCl}/a_0	RCCSD	RCCSD[T]	RCCSD(T)	RCCSD-T
cc-pVDZ	2.888	1.276	1.094	1.098	1.102
cc-pVTZ	2.875	1.264	1.018	1.020	1.024
cc-pVQZ	2.873	1.235	0.9694	0.9715	0.9749
cc-pV5Z	2.871	1.233	0.9588	0.9608	0.9642
aug-cc-pVDZ	2.894	1.139	0.9291	0.9322	0.9370
aug-cc-pVTZ − f(Cl)	2.875	1.193	0.9292	0.9319	0.9360
aug-cc-pVTZ	2.874	1.199	0.9348	0.9375	0.9416
aug-cc-pVQZ − g(Cl)	2.874	1.205	0.9319	0.9342	0.9379
aug-cc-pVQZ	2.874[a]	1.207	0.9328	0.9352	0.9389

[a] aug-cc-pVTZ geometry used.

little effect on the reactivity for translational energies important to the thermal rate coefficient, although the $^2\Pi$ surface should become more important at higher energies.

If the constraint of collinearity is relaxed, the ground state barrier height E_b drops by 0.0727 eV at a bond angle $\theta = 137°$ (see Table 4). This is consistent with the PES of Garrett *et al.*[12] who computed six non-collinear points. A scaled and fitted version of their surface (denoted sf-PolCI) has $E_b =$ 0.326 eV located at $r_{HCl} = 2.784\ a_0$ with $\theta = 161.4°$.[13] A similar study of the TS was performed by Vincent *et al.*[9] There is generally good agreement with the barrier heights and geometries of ref. 9, *e.g.* $E_b = 0.621$ eV for MRCI ($E_b =$ 0.433 eV including the Davidson correction), with $r_{HCl} = 2.823$ a_0, $\theta = 148°$ and $E_b = 0.537$ eV, $r_{HCl} = 2.806\ a_0$, $\theta = 137°$ for UMP2(I). These *ab initio* results contrast with several LEPS PESs[15,18] all of which have collinear TSs.

It has been suggested that the C_{2v} TS might not be the true TS; rather there are two asymmetric TSs situated either side of this C_{2v} minimum.[9,35] However, we find on fitting energies close to the C_{2v} TS (calculated using the procedure described in Section II) to a second degree polynomial, that the harmonic wavenumber constant associated with the asymmetric stretching motion is imaginary, which implies there is indeed a saddle point at C_{2v} ($\nu_{ss} = 210 \pm 10$ cm^{-1}, $\nu_b = 1114 \pm 50$ cm^{-1}, $\nu_{as} = 1575i \pm 100i$ cm^{-1}, using $m_{Cl} = 34.969$ u and $m_H = 1.0079$ u).

To obtain a definitive value for the ground state E_b a full configuration-interaction (FCI) calculation in a complete basis set would be necessary, which is of course impossible. If it is assumed that RCCSD-T is a good approximation to FCI, then studying the results from a sequence of basis sets will give us an estimate of E_b in the limit of a complete basis set. Our results show that even using very large basis sets such as aug-cc-pVQZ, the value of E_b is not completely converged. In the limit of a complete basis set, the results in Table 4 suggest that $E_b = 0.35$–0.40 eV would be obtained. An interesting point to note is that removal of the diffuse functions from the basis sets in Tables 2–4, contrary to expectation, usually results in a lower E_b. This can be attributed to the contraction of the p functions in the ClHCl complex, which probably results in reduced overlap of the atomic orbitals and hence less intermolecular repulsion. Another contributing factor to the effect of diffuse functions on E_b is that the p orbitals in the isolated Cl atom are rather diffuse, so that exclusion of the diffuse atomic orbitals raises the asymptotic energy, hence reducing E_b.

The collinear results (Tables 2 and 3) show the importance of including triple excitations, particularly for the excited states. For the $^2\Sigma_u^+$ state the drop in E_b from the RCCSD to RCCSD-T is 0.11–0.13 eV and for the $^2\Pi_g$ state it is $\approx$0.26 eV, though these differences may be slightly over-estimated given that the geometries are optimized at the RCCSD-T level.

As one might expect, the differences in E_bs obtained from the three different triples *ansätze* in Tables 2–4 are very small (<0.009 eV); this is because the *ansätze* only differ in fifth order perturbation theory. Detailed comparison of the different triples corrections is limited because the geometries were optimized at the RCCSD-T level. However, it should be noted that the RCCSD-T correction results in an E_b that is nearly always greater than those from RCCSD[T] or RCCSD(T).

III Diabatic transformation

In this section we present the transformations of the PESs from the adiabatic basis to a diabatic basis. The electronic states in a diabatic basis, χ^d_{11}, χ^d_{22}, are obtained by a unitary transformation from those in the adiabatic basis:

$$\begin{pmatrix} \chi^d_{11} \\ \chi^d_{22} \end{pmatrix} = \begin{pmatrix} \cos\alpha & \sin\alpha \\ -\sin\alpha & \cos\alpha \end{pmatrix} \begin{pmatrix} \Psi^a_1 \\ \Psi^a_2 \end{pmatrix} \quad (1)$$

where α is the 'mixing angle', which is a function of the three

Table 4 Height (eV) and position of the barrier for the $1\,^2B_1$ state of ClHCl, which is the ground state of the bent symmetric, C_{2v}, molecule, for different basis sets. The geometries are optimized at the RCCSD-T level. Also included is the dipole polarizability of ClHCl, calculated at the RCCSD-T level (α' is the polarizability volume)

Basis	r_{HCl}/a_0	θ/degrees	RCCSD	RCCSD[T]	RCCSD(T)	RCCSD-T	α'/a_0^3
cc-pVDZ	2.833	142	0.6487	0.5581	0.5591	0.5610	20.871
cc-pVTZ	2.824	139	0.6221	0.4859	0.4847	0.4878	25.354
cc-pVQZ	2.827	135	0.5975	0.4397	0.4412	0.4431	30.209
aug-cc-pVDZ	2.847	139	0.5901	0.4737	0.4716	0.4757	33.620
aug-cc-pVTZ − f(Cl)	2.826	139	0.5747	0.4262	0.4244	0.4283	34.919
aug-cc-pVTZ	2.829	137	0.5850	0.4321	0.4341	0.4361	35.361
aug-cc-pVQZ − g(Cl)	2.824	137	0.5761	0.4176	0.4158	0.4195	35.926
aug-cc-pVQZ	2.829[a]	137[a]	0.5766	0.4156	0.4174	0.4193	36.054

[a] aug-cc-pVTZ geometry used.

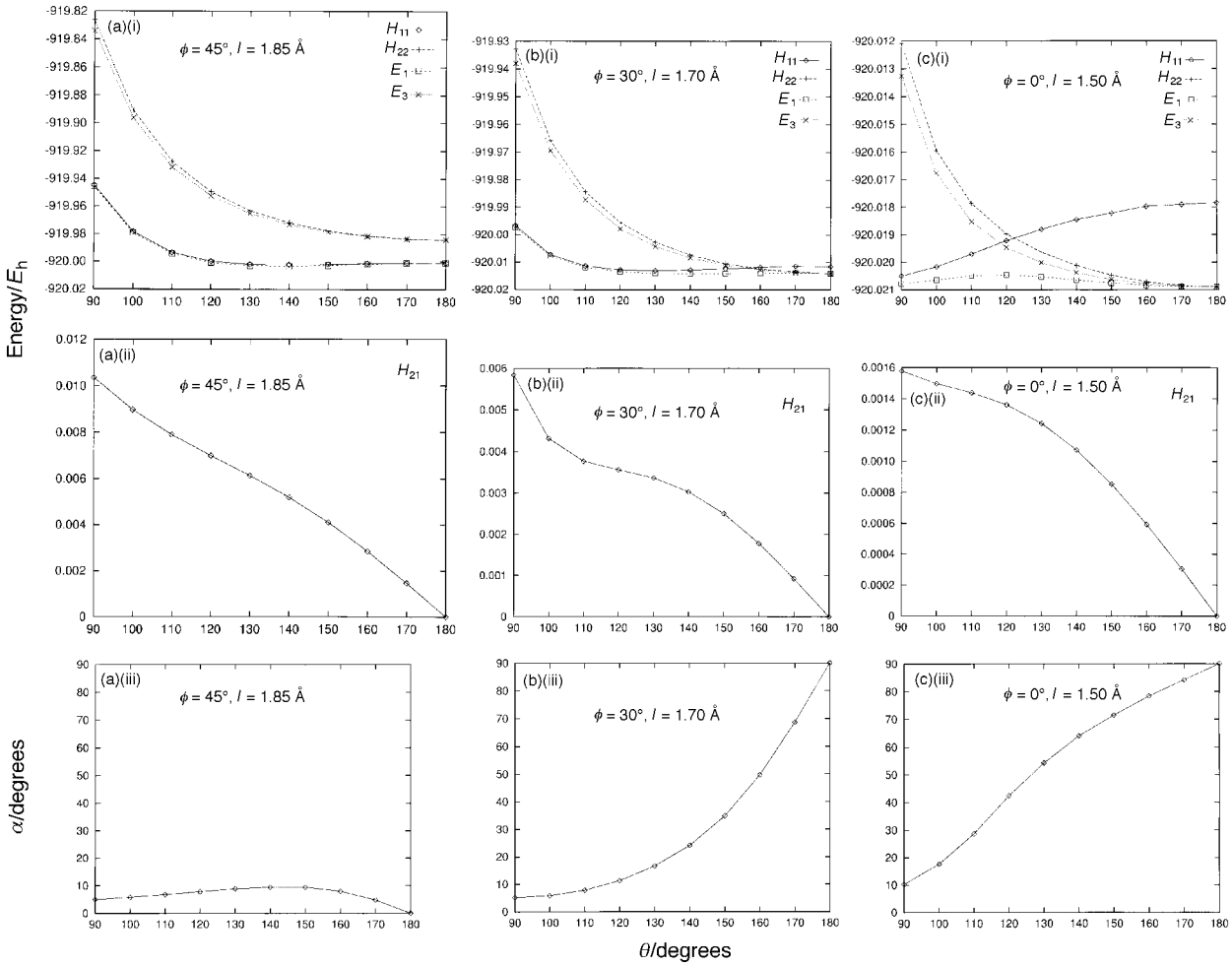

Fig. 1 (a) (i) RCCSD-T adiabatic energies, E_1 and E_3, together with the RCCSD-T diabatic energies, $H_{11}^{\text{RCCSD-T}}$ and $H_{22}^{\text{RCCSD-T}}$ *versus* ClHCl bond angle, θ. (ii) MRCI coupling diabatic potential, H_{21}^{MRCI} *versus* θ. (iii) RCCSD-T mixing angle, $\alpha^{\text{RCCSD-T}}$ *versus* θ. The values of the parameters of the rotated Morse cubic spline function for graphs (i)–(iii) are $\phi = 45°$, $l = 1.85$ Å. (b) The same as (a), except $\phi = 30°$, $l = 1.70$ Å, (c) The same as (a), except $\phi = 0°$, $l = 1.50$ Å. The *ab initio* points have been joined by straight lines and do not represent the fitted PESs.

nuclear coordinates. The resulting diabatic states are no longer eigenvectors of the electronic Hamiltonian, which is therefore not diagonal; rather it has elements

$$H_{11} = \cos^2 \alpha E_1 + \sin^2 \alpha E_2$$
$$H_{22} = \sin^2 \alpha E_1 + \cos^2 \alpha E_2$$
$$H_{21} = H_{12} = (E_2 - E_1)\cos \alpha \sin \alpha \qquad (2)$$

There are several ways to achieve this transformation. The most rigorous, and computationally expensive, is by integration of the non-adiabatic coupling matrix elements (NACMEs).[36–38] We will use an approximate, and computationally less demanding, method which exploits molecular properties to characterize the diabatic transformation; in previous applications this approach has performed well.[39–44] The reasoning behind it is that as the adiabatic wavefunctions in the vicinity of the state-crossing mix, and eventually interchange their characters, the molecular properties will reflect this character transition. The particular molecular property used to construct the transformation to the diabatic basis is the transition angular momentum connecting the A'' state and the two states of A′ symmetry.[45–47]

A Transformation to a diabatic basis using the transition angular momentum operator

The method we employ to extract α from molecular properties uses matrix elements of the form $\langle \Psi_3^a | \hat{P} | \Psi_1^a \rangle$ and $\langle \Psi_3^a | \hat{P} | \Psi_2^a \rangle$, where Ψ_3^a is a third electronic state not involved in the electronic-mixing, and the Dirac brackets denote integration over electronic coordinates. These matrix elements can be expressed in terms of the diabatic states, using the inverse of the transformation given in eqn. (1),

$$\langle \Psi_3^a | \hat{P} | \Psi_1^a \rangle = \cos \alpha \langle \Psi_3^a | \hat{P} | \chi_{11}^d \rangle - \sin \alpha \langle \Psi_3^a | \hat{P} | \chi_{22}^d \rangle \qquad (3)$$

and

$$\langle \Psi_3^a | \hat{P} | \Psi_2^a \rangle = \sin \alpha \langle \Psi_3^a | \hat{P} | \chi_{11}^d \rangle + \cos \alpha \langle \Psi_3^a | \hat{P} | \chi_{22}^d \rangle \qquad (4)$$

If the matrix elements involving the diabatic states have known values, then it is possible to gain information about the value of α. In the case under consideration χ_{11}^d can be loosely identified with the $^2\Sigma^+$ state and χ_{22}^a with the $^2\Pi$ state. If then Ψ_3^a is taken to be the $^2A''$ state, which corresponds to the other component of the $^2\Pi$ state at collinear geometries, and the operator $\hat{P} = \hat{L}_x$ (which is parallel to the molecular axis for collinear ClHCl), eqn. (3) and (4) can be written for the $1\,^2A'$ state

$$\langle {}^2A'' | \hat{L}_x | 1\,^2A' \rangle = \cos \alpha \langle {}^2A'' | \hat{L}_x | {}^2\Sigma^+ \rangle - \sin \alpha \langle {}^2A'' | \hat{L}_x | {}^2\Pi \rangle \qquad (5)$$

and similarly for the $2\,^2A'$ state,

$$\langle {}^2A'' | \hat{L}_x | 2\,^2A' \rangle = \sin \alpha \langle {}^2A'' | \hat{L}_x | {}^2\Sigma^+ \rangle + \cos \alpha \langle {}^2A'' | \hat{L}_x | {}^2\Pi \rangle \qquad (6)$$

The assumption is then made that $\langle {}^2A'' | \hat{L}_x | {}^2\Sigma^+ \rangle = 0$ and

$|\langle {}^2A''|\hat{L}_x|{}^2\Pi\rangle| = 1$ for all geometries (not just at collinearity, where the assumption is true) so that α can be approximated as

$$\alpha = \arctan\left(\frac{|\langle {}^2A''|\hat{L}_x|1\,{}^2A'\rangle|}{|\langle {}^2A''|\hat{L}_x|2\,{}^2A'\rangle|}\right) \quad (7)$$

where $0 \leqslant \alpha \leqslant \pi/2$.

B Procedure for combining the RCCSD-T and MRCI results

As already mentioned in Section II, it is necessary to combine results at the RCCSD-T level with those obtained at the MRCI level. This is due to the single reference nature of the RCCSD-T technique, which means that no information about the $2\,{}^2A'$ state can be gained, except at the collinear configuration. We used the following procedure:

1. H_{21}^{MRCI}, H_{22}^{MRCI} and H_{11}^{MRCI} are calculated at the MRCI level, using eqn. (2) and (7), as outlined in the previous sections (Sections III and IIIA).

2. $(H_{22} - H_{11})^{\mathrm{RCCSD\text{-}T}}$ is determined such that: (a) It has the same variation with the ClHCl bond angle, θ, as $(H_{22} - H_{11})^{\mathrm{MRCI}}$. (b) It agrees with RCCSD-T for $\theta = 180°$.

This results in the following expression for $(H_{22} - H_{11})^{\mathrm{RCCSD\text{-}T}}(\theta)$:

$$(H_{22} - H_{11})^{\mathrm{RCCSD\text{-}T}}(\theta) = (H_{22} - H_{11})^{\mathrm{MRCI}}(\theta) - (H_{22} - H_{11})^{\mathrm{MRCI}}(180°) + (H_{22} - H_{11})^{\mathrm{RCCSD\text{-}T}}(180°) \quad (8)$$

3. This expression for $(H_{22} - H_{11})^{\mathrm{RCCSD\text{-}T}}(\theta)$ is used together with the coupling potential H_{21}^{MRCI} to obtain a new RCCSD-T mixing angle,

$$\alpha^{\mathrm{RCCSD\text{-}T}} = \frac{1}{2}\arctan\left(\frac{2H_{21}^{\mathrm{MRCI}}}{(H_{22} - H_{11})^{\mathrm{RCCSD\text{-}T}}(\theta)}\right) \quad (9)$$

The value of $\alpha^{\mathrm{RCCSD\text{-}T}}$ is forced to lie between 0 and $\pi/2$. Note also that $H_{21}^{\mathrm{MRCI}}(\theta) = 0$ for $\theta = \pi$.

4. The new RCCSD-T diabatic states are then evaluated by substituting $\alpha^{\mathrm{RCCSD\text{-}T}}$ into

$$H_{11}^{\mathrm{RCCSD\text{-}T}} = E_1^{\mathrm{RCCSD\text{-}T}} + H_{21}^{\mathrm{MRCI}} \tan \alpha^{\mathrm{RCCSD\text{-}T}} \quad (10)$$

$$H_{22}^{\mathrm{RCCSD\text{-}T}} = E_1^{\mathrm{RCCSD\text{-}T}} + H_{21}^{\mathrm{MRCI}} \cot \alpha^{\mathrm{RCCSD\text{-}T}} \quad (11)$$

Note that H_{11}^{X}, H_{22}^{X}, with X = MRCI, RCCSD-T and H_{21}^{MRCI}, $E_1^{\mathrm{RCCSD\text{-}T}}$, $\alpha^{\mathrm{RCCSD\text{-}T}}$ are all functions of the three nuclear coordinates.

C MRCI and RCCSD-T results

Fig. 1 displays the RCCSD-T adiabatic energies E_1 and E_3 and diabatic energies $H_{11}^{\mathrm{RCCSD\text{-}T}}$, $H_{22}^{\mathrm{RCCSD\text{-}T}}$, H_{21}^{MRCI}, as well as $\alpha^{\mathrm{RCCSD\text{-}T}}$, all as functions of θ for three different cuts through the potentials. The cuts correspond to different choices for the parameters l, ϕ of the rotated-Morse cubic-spline (RMCS) functions defined in Sections IV and V. For a swing angle of $\phi = 45°$ (and $l = 1.85$ Å), Fig. 1[(a)(i)], the energy of the ground adiabatic state E_1 is seen to be very close to the H_{11} diabatic state energy for all θ. Note that $\phi = 45°$ corresponds to C_{2v} geometries; for this case there is no crossing of the 'Σ-like' and 'Π-like' diabatic curves, as a result for $\theta = 180°$, we have $H_{11}^{\mathrm{RCCSD\text{-}T}} = E_1$ and $H_{22}^{\mathrm{RCCSD\text{-}T}} = E_3$. Also the 'Σ-like' $H_{11}^{\mathrm{RCCSD\text{-}T}}$ curve has the lower diabatic energy for all values of θ and l. For a swing angle of $\phi = 30°$ (and $l = 1.70$ Å), Fig. 1[(b)(i)], the energy of the ground adiabatic state E_1 has 'Σ-like' character for $\theta \lesssim 150°$ but switches to 'Π-like' character at larger θ. As a result, at $\theta = 180°$, we have $E_1 = E_3 = H_{22}^{\mathrm{RCCSD\text{-}T}}$ (and $H_{11}^{\mathrm{RCCSD\text{-}T}} = E_2$). Similar behaviour occurs for the case $\phi = 0°$ ($l = 1.50$ Å), Fig. 1[(c)(i)], except that the crossing between the diabatic states occurs at $\theta \approx 120°$, and the crossing takes place more slowly as can be appreciated by comparing the rate of variation of the mixing angles presented in Fig. 1[(b)(iii) and (c)(iii)]. Notice also that as we decrease ϕ in Fig. 1[(a)(ii)–(c)(ii)], H_{21}^{MRCI} becomes smaller for a given $\theta(\neq 180°)$, since the diabatic curves $H_{11}^{\mathrm{RCCSD\text{-}T}}$ and $H_{22}^{\mathrm{RCCSD\text{-}T}}$ move closer together as they approach their asymptotic values.

IV Grid employed for the *ab initio* computation of the potential energy surfaces

In order to produce a set of global surfaces for the Cl + HCl reaction, it is necessary to compute the energies of the $1\,{}^2A'$, $2\,{}^2A'$ and ${}^2A''$ states, using the *ab initio* procedure described in Section II, at a large number of points spanning the three nuclear coordinates (l, ϕ, θ). The coordinates l and ϕ are defined *via* the following relationships:

$$l = [(r_{\mathrm{HCl}}^* - r_{\mathrm{HCl}})^2 + (r_{\mathrm{ClH}}^* - r_{\mathrm{ClH}})^2]^{1/2} \quad (12)$$

$$\phi = \arctan\left(\frac{r_{\mathrm{ClH}}^* - r_{\mathrm{ClH}}}{r_{\mathrm{HCl}}^* - r_{\mathrm{HCl}}}\right) \quad (13)$$

where $r_{\mathrm{HCl}}^* = r_{\mathrm{ClH}}^* = 5.304\ a_0$ and is the location of the 'swing point', which defines the origin of the (l, ϕ) coordinates.

As mentioned in Section III, we fitted the points using the RMCS procedure (described in more detail in Section VA). This determines, at least partially, the location of the grid points for the *ab initio* computations. We chose the following values for ϕ and l:

$\phi = 45°$ with $l = 2.10, 1.85, 1.65$ Å

$\phi = 40°$ with $l = 2.05, 1.85, 1.65$ Å

$\phi = 35°$ with $l = 2.00, 1.80, 1.60$ Å

$\phi = 30°$ with $l = 1.90, 1.70, 1.50$ Å

$\phi = 15°$ with $l = 1.80, 1.60, 1.40$ Å

$\phi = 0°$ with $l = 1.70, 1.50, 1.30$ Å

Finally we varied the ClHCl bond angle, θ, over the range 90–180° in 10° steps. Thus we used a grid of 180 points for the *ab initio* calculations.

V Fitting of the *ab initio* energies to smooth functions

We have four PESs to be fitted: the ${}^2A''$ state, E_3; the 'Σ-like' diabatic surface, H_{11}; the 'Π-like' diabatic surface, H_{22}; and the diabatic coupling potential, H_{21}. (H_{11} *etc.* rather than $H_{11}^{\mathrm{RCCSD\text{-}T}}$ *etc.* are written from now on.) We prefer to fit the diabatic surfaces, H_{11} and H_{22}, rather than the adiabatic surfaces, E_1 and E_2, since the former are expected to vary more smoothly with nuclear configuration than the latter. Diabatic surfaces are also more convenient to use in dynamical calculations than are adiabatic surfaces together with the NACMEs.

The three potential surfaces, E_3, H_{11} and H_{22} were fitted using a RMCS function, described in the next section (Section VA). However, the form of the coupling potential, H_{21}, is probably less suited for fitting to such a function. Instead the following procedure was used, in which H_{21} is fitted to the sinusoidal form

$$[a(\phi, \theta)l^3 + b(\phi, \theta)l^2 + c(\phi, \theta)l]\sin\theta \quad (14)$$

at each value of ϕ and θ on the grid. The parameters $a(\phi, \theta)$, $b(\phi, \theta)$ and $c(\phi, \theta)$ are then interpolated by a 2D bicubic spline to yield smooth functions of ϕ and θ.

A Rotated-Morse cubic-spline function

The rotated Morse curve (RMC) function of Wall and Porter[48] can be considered a generalization of a Morse diatomic potential to a bimolecular exchange reaction. It is

based on the observation that the PES can be viewed as a rotation of a diatomic potential about a 'swing point'. The location of the swing point remains somewhat arbitrary although methods have been proposed for the selection of the best point.[49] Once the swing point has been chosen, any position on the PES for a fixed value of the ABC bond angle θ is given by the swing radius, l, and the swing angle, ϕ.

The RMC function for a general exchange reaction A + BC → AB + C can be written:[50,51]

$$V(l, \phi, \theta) = D(\phi, \theta)[(1 - \exp\{\beta(\phi, \theta)[l - l_e(\phi, \theta)]\})^2 - 1] + D_{BC} \quad (15)$$

where D_{BC} is the BC dissociation energy and $D(\phi, \theta)$, $\beta(\phi, \theta)$ and $l_e(\phi, \theta)$ are the three Morse parameters. These Morse parameters are first obtained on a grid of ϕ_i, θ_j and then smoothly interpolated using a 2D bicubic spline fit. This procedure is called the RMCS method.[52]

We used a value of D_{HCl} which is taken from the BCMR LEPS surface,[4] and has the value 4.618 eV. All the *ab initio* energies are measured relative to the energy of HCl(r^e_{HCl} = 2.417 a_0) + Cl, which is our calculated value for the classical minimum of the HCl potential.

B Global potential energy surfaces

Although we have calculated *ab initio* energies at 180 grid points for a wide range of geometries, the points do not extend very far into the asymptotic regions nor to ClHCl bond angles $\theta < 90°$. It is therefore necessary to combine our *ab initio* PESs with potential functions valid at long range, and/or $\theta < 90°$, in order to obtain a set of global PESs. We followed the procedure of Maierle *et al.*,[4] whose paper should be consulted for further details. It should be emphasised however that our work differs from that presented by Maierle *et al.*[4] in that we have fully *ab initio* surfaces for H_{22} and H_{21} in the strong interaction region, as well as for H_{11} and E_3.

Long-range potentials. Dubernet and Hutson[2] (DH) have studied the van der Waals interaction of Cl with HCl, *i.e.* the long-range part of the ClHCl PESs. Their potential is constructed using physical intuition and analogies with Ar–HCl, Ar–Cl and Ar–Ar potentials, plus the addition of a term describing the interaction of the Cl quadrupole with the HCl multipoles. Their potential assumes that the HCl molecule is rigid, and depends only on the R and γ Jacobi coordinates. It is therefore necessary to augment the DH potential so that it also depends on the HCl bond length r_{HCl}. This is achieved by symmetrically adding a Morse function, whose parameters are taken from the BCMR LEPS PES.[18] In addition, the DH potential depends on the angles θ_a and ϕ_a, which specify the orientation of the singly occupied p orbital on Cl relative to the plane of the three atoms. Thus, this augmented DH potential provides a representation of the E_3, H_{11}, H_{22} and H_{21} PESs at long range.

We combined the augmented DH potentials, which are only intended to be accurate at long-range, with the *ab initio* PESs using the simple switching function:

$$V_i = V_{ab\ initio,\ i} S + V_{DH,\ i}(1 - S) \quad (16)$$

where $V_{ab\ initio}$ refers to our calculated *ab initio* PESs, V_{DH} refers to the Dubernet and Hutson PESs, S is a switching function, and the index i runs over the four different PESs: E_3, H_{11}, H_{22} and H_{21}. The switching function is given by

$$S(r_{HCl}, r_{ClH}) = \tfrac{1}{4}\{1 - \tanh[\zeta(r_{HCl} - r^s_{HCl})]\} \times \{1 - \tanh[\zeta(r_{ClH} - r^s_{ClH})]\} \quad (17)$$

where $r^s_{HCl} = r^s_{ClH} = 4.3\ a_0$ and $\zeta = 5\ a_0^{-1}$.

Potentials for small ClHCl bond angles. For $\theta < 90°$, the adiabatic PESs are very repulsive, so this region of configuration space is unlikely to have a significant effect on the dynamics, at least at low collision energies. However it is still convenient to have PESs defined for $\theta < 90°$. This can be achieved by switching to the BCMR LEPS PES for H_{11}, and to a second LEPS PES for $(E_3 + H_{22})/2$, using a hyperbolic tangent function, with a switching ClHCl bond angle of 110 degrees, and a switching parameter of 0.2 degrees^{-1}. This second LEPS PES is more repulsive than the BCMR LEPS PES, so although it used the same parameters for the diatomic fragments, the Sato parameter was chosen to be −0.115, since this value provides a smooth extrapolation from the *ab initio* data. It is easily seen in Fig. 1 that the 'Π-like' diabatic curves, H_{22}, are much more repulsive than the 'Σ-like' diabatic curves, H_{11}, so that it is necessary to use a LEPS PES significantly more repulsive than BCMR (which is used for H_{11}) for the extrapolation of $(E_3 + H_{22})/2$ into the $\theta < 90°$ region. H_{21} and $(E_3 - H_{22})/2$ were extended to $\theta < 90°$ by switching to the DH potential, using the switching function just described.

VI Properties of the global potential energy surfaces

The positions and heights of the barriers for the $^2\Sigma_u^+$, $^2\Pi_g$, $1\,^2B_1$ adiabatic and the H_{11} and H_{22} diabatic states, derived from the fitted PESs, are shown in Table 5, together with the harmonic wavenumber constants. They are in good agreement with the results from the convergence tests (Tables 2, 3 and 4). In particular, the TS for the $1\,^2A'$ ($1\,^2B_1$) surface occurs at $\theta = 137.7°$, $r_{HCl} = 2.826\ a_0$, which is only 0.0646 eV lower than the height of the collinear ClHCl stationary point, highlighting the fact that the bending potential is rather flat.

Contour plots of the PESs for collinear ClHCl are shown in Fig. 2. The conical intersection seam between the $^2\Sigma^+$ and $^2\Pi$ states in Fig. 2(a) and (b) is similar to that presented by Maierle *et al.* [see Fig. 4(a) and (b) of ref. 4]. The van der Waals wells on the H_{22} surface [Fig. 2(b)] and the E_1 surface [Fig. 2(c)] are centred around $r_{HCl} = 5\ a_0$, and are clearly visible. Similar contour plots for ClHCl with $\theta = 140°$ are shown in Fig. 3. The intersection seam in Fig. 3(a) and (b)

Table 5 Barrier heights and positions, together with harmonic wavenumber constants for ν_{ss}, the symmetric stretching coordinate, ν_{as}, the asymmetric stretching coordinate and ν_b, the bending coordinate, for symmetric ClHCl on the fitted PESs. Results are presented for adiabatic and diabatic states, for collinear and, where they differ, bent geometries

State	r_{HCl}/a_0	θ/degrees	Barrier height/eV	ν_{as}/cm^{-1}	ν_b/cm^{-1}	ν_{ss}/cm^{-1}
$^2\Sigma_u^+(E_1)$	2.799	180	0.4924	1829i	390i	359
$^2\Pi_g(E_2)$	2.870	180	0.9419	4567i	661	353
$^2\Pi_g(E_3)$	2.870	180	0.9419	4567i	455	353
H_{11}	2.799	180	0.4924	1829i	390i	359
H_{22}	2.870	180	0.9419	4567i	553	353
H_{11}	2.830	138.5	0.4521	1702i	1053	196
$1\,^2B_1$	2.826	137.7	0.4278	1673i	1099	206

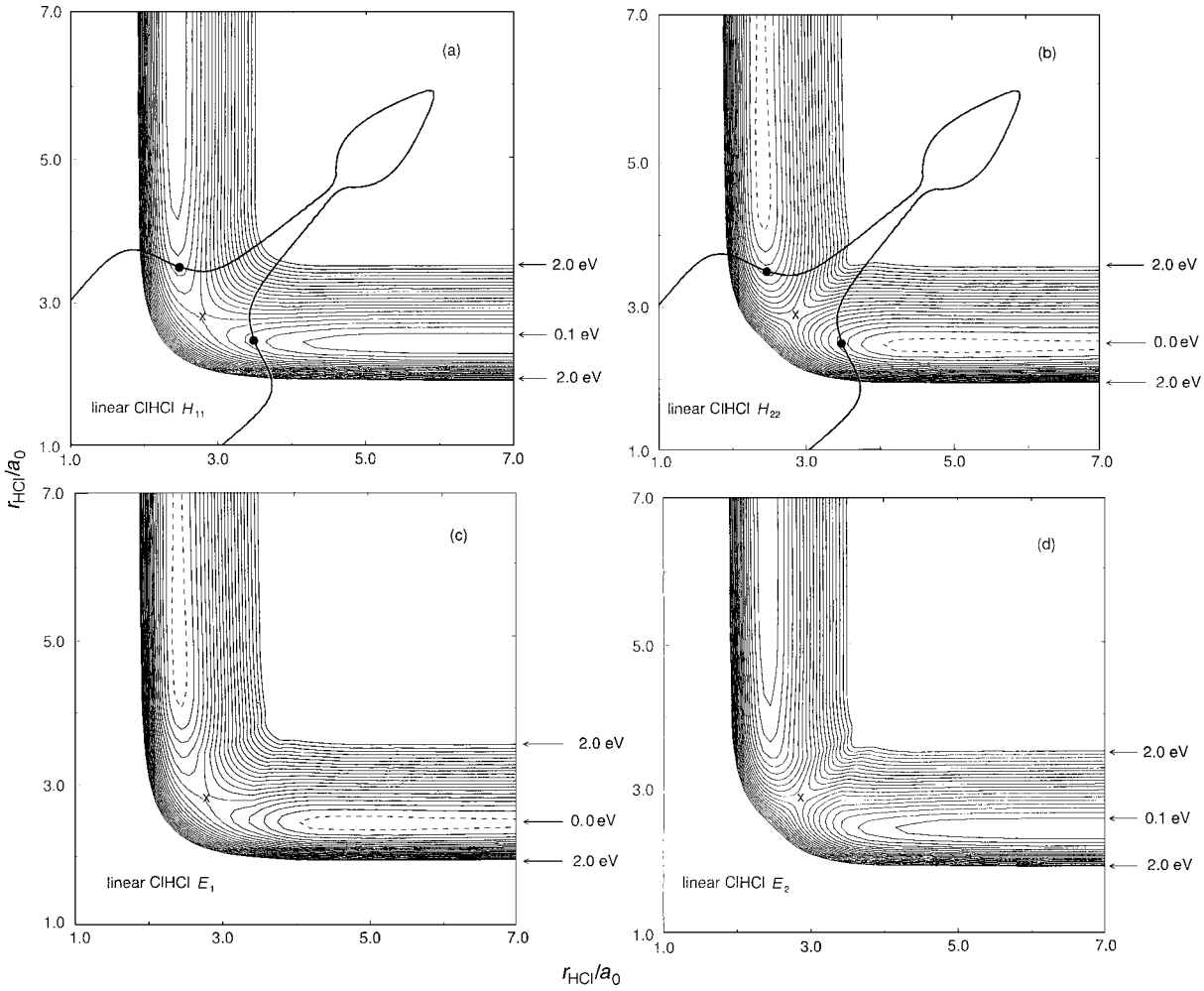

Fig. 2 Contour plots of the global potential energy surfaces for collinear ClHCl as a function of the two HCl distances. (a) Σ diabatic potential, H_{11}. (b) Π diabatic potential, H_{22}, which is degenerate with the excited $^2A''$, E_3. (c) Ground-state adiabatic potential $1\,^2A'$, E_1. (d) Excited adiabatic potential $2\,^2A'$, E_2. The contour interval is 0.1 eV, with the lowest contour being at 0.0 eV in (b) and (c), and 0.1 eV in (a) and (d). Positive energy contours (———) and the zero energy contour (– – – –). In (a) and (b), the intersection seam, which is not an energy contour, is shown as a thick solid line with (●) denoting the lowest energies of the seam. (×) marks the position of a stationary point.

between the two diabatic surfaces has moved outwards to larger r_{HCl} and r_{ClH} distances compared to the collinear case; the adiabatic surfaces [Fig. 3(c) and (d)] are smoother than at collinearity, as the crossing between the diabatic states becomes broader away from $\theta = 180°$. The differences between H_{22} and E_3 are small [compare Fig. 3(b) and (e)], which is also true for the DH potential. The long-range parts of the PESs are essentially identical to those presented by Maierle *et al.* (see Fig. 5 of ref. 4). It is important to note that the contour plots displayed in Fig. 2 and 3 are all smooth in the switching region between the *ab initio* RMCS functions and the semi-empirical DH potentials, which is also the case at other bond angles.

Fig. 4(a) shows the minimum energy profiles for H_{11} and H_{22}. The swing angle ϕ is used as a reaction coordinate. For a fixed ϕ, we have minimized H_{11} and H_{22} with respect to θ and l. The profiles are seen to cross about half way up the barrier of the 'Σ-like' diabat, H_{11}. The TS for the 'Π-like' diabat, H_{22}, is about twice as high as that for the 'Σ-like' diabat, H_{11}. There are van der Waals wells on the H_{22} curve, whilst the H_{11} curve appears to be always repulsive (in fact van der Waals wells do exist on the $^2\Sigma^+$ state,[2,4] but they are outside the coordinate range of Fig. 4, occurring at larger r_{HCl} and r_{ClH} distances). The corresponding curves for E_1, E_2 and E_3 are displayed in Fig. 4(b); the curves for E_1 and E_2 'avoid' each other around the point where the 'Σ-like' and 'Π-like' diabats cross. It is clear that the ground adiabatic surface is 'Π-like' at long-range, but 'Σ-like' in the region of the TS.

VII Conclusions

Whilst dynamical calculations on coupled PESs are becoming routine, the *ab initio* calulation of coupled PESs is still a difficult task, rarely undertaken. In this paper we have computed the three relevant surfaces and the diabatic coupling for the $Cl(^2P) + HCl \rightarrow ClH + Cl(^2P)$ reaction, which are being used in dynamical calculations.

The PESs presented in this work are better than previous surfaces in several ways:‖ 1. A *complete* set of PESs necessary for the description of $Cl(^2P) + HCl$ has been calculated, including the non-adiabatic interaction between the two states of A′ symmetry. 2. The computations have been performed at the RCCSD-T and MRCI levels of theory, thereby including a large proportion of the dynamic correlation energy. 3. A wide range of bond angles have been included, with 180 grid points spread across the PESs.

The work presented in this paper has not taken into account any relativistic effects. It is known that the spin–orbit (SO) splitting of Cl is 0.109 eV. This splits the degeneracy of the $^2\Pi$ state into $^2\Pi_{3/2}$ and $^2\Pi_{1/2}$, lowering the energy of the $Cl(^2P_{3/2})$ asymptote by 1/3 of the SO splitting. It therefore also increases the height of the reaction barrier, since to first order, the $^2\Sigma_{1/2}{}^+$ state in the TS region is not affected by SO coupling, due to the quenching of the electronic orbital angular momentum. Thus, relativistic effects can influence the

‖ These PESs can be obtained from G.C.S.: schatz@chem.nwu.edu.

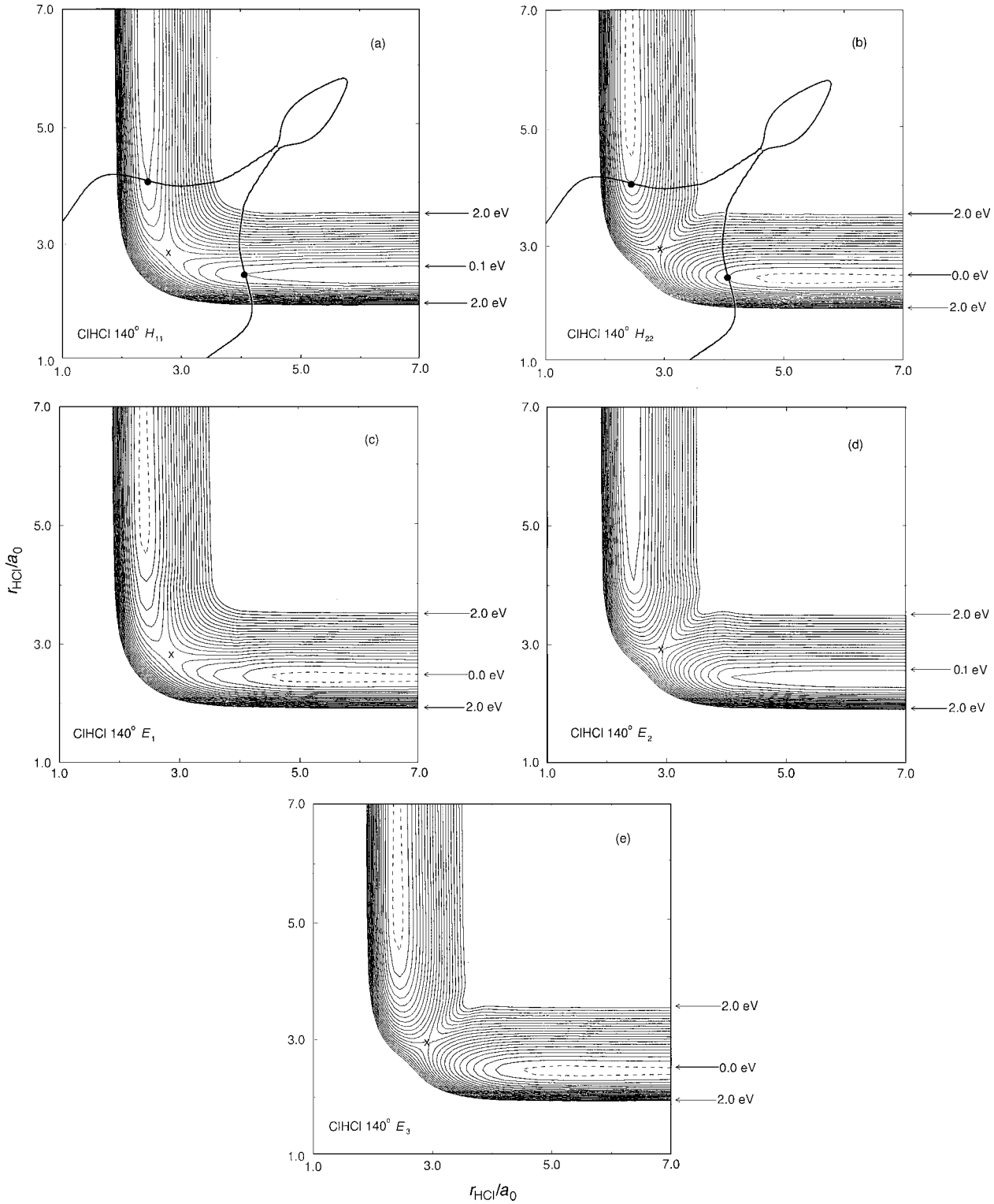

Fig. 3 Same as Fig. 2 except for a ClHCl bond angle of $\theta = 140°$. (a) 'Σ-like' diabatic potential, H_{11}. (b) 'Π-like' diabatic potential, H_{22}. (c) Ground-state adiabatic potential $1\,^2A'$, E_1. (d) Excited adiabatic potential $2\,^2A'$, E_2. (e) Excited adiabatic potential $^2A''$, E_3. The contour interval is 0.1 eV, with the lowest contour being at 0.0 eV in (b), (c) and (e), and 0.1 eV in (a) and (d). Positive energy contours (———) and the zero energy contour (– – – –). In (a) and (b), the intersection seam, which is not an energy contour, is shown as a thick solid line with (●) denoting the lowest energies of the seam. (×) marks the position of a stationary point.

reaction dynamics, and therefore PESs should be generated which include these effects. Visscher and Dyall[53] have investigated whether relativistic effects significantly influence the lower barrier height of ClHCl. Scalar relativistic effects were found to lower the barrier height by 0.005 eV while spin–orbit effects were found to raise the barrier height by 0.026 eV; the overall increase in the barrier height being 0.021 eV. This is in fair agreement with a shift of 0.032 eV from a perturbative treatment of the spin–orbit coupling, which assumes the SO coupling constant is independent of geometry.[3,4] There are likely to be larger errors than this in our computed surfaces, arising, for example, from an incomplete 1-electron basis set, so the very large effort required to include SO coupling is probably not justified at the present time.

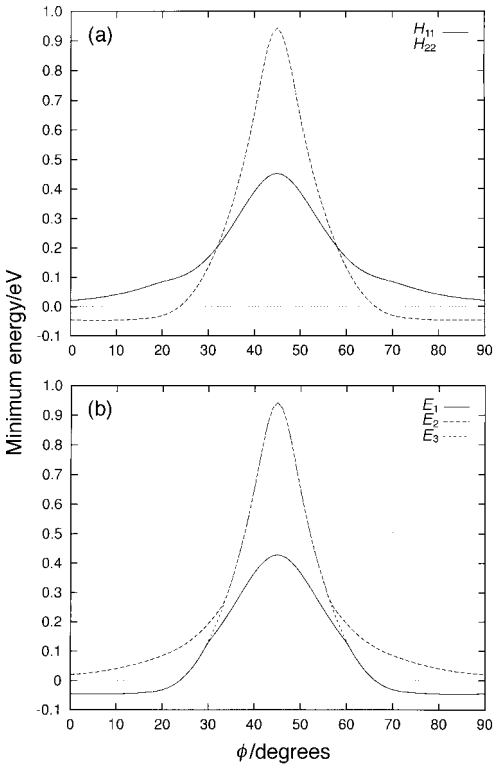

Fig. 4 (a) Minimum energy profiles for the diabatic surfaces, H_{11} and H_{22}. (b) Minimum energy profiles for the adiabatic surfaces, E_1, E_2 and E_3. The swing angle ϕ is used as a reaction coordinate.

Acknowledgements

A.J.D. and J.N.L.C. thank Dr. M. A. Vincent (University of Manchester) for helpful conversations. The work of A.J.D., J.N.L.C., N.A.B. and P.J.K. was supported by the UK Engineering and Physical Sciences Research Council. Work by G.C.S. was supported by the US Department of Energy, Office of Basic Energy Sciences, Division of Chemical Sciences under contract No. W-31-109-ENG-38.

References

1 G. C. Schatz, D. Sokolovski and J. N. L. Connor, in *Advances in Molecular Vibrations and Collision Dynamics*, ed. J. M. Bowman, JAI Press, Greenwich, CT, 1994, vol. 2B, pp. 1–26.
2 M-L. Dubernet and J. M. Hutson, *J. Phys. Chem.*, 1994, **98**, 5844.
3 G. C. Schatz, *J. Phys. Chem.*, 1995, **99**, 7522.
4 C. S. Maierle, G. C. Schatz, M. S. Gordon, P. McCabe and J. N. L. Connor, *J. Chem. Soc., Faraday Trans.*, 1997, **93**, 709.
5 G. C. Schatz, P. McCabe and J. N. L. Connor, *Faraday Discuss.*, 1998, **110**, 139.
6 P. Botschwina and W. Meyer, *Chem. Phys. Lett.*, 1976, **44**, 449.
7 K. Yamashita and K. Morokuma, *J. Chem. Phys.*, 1990, **93**, 3716.
8 K. Yamashita and K. Morokuma, *J. Chem. Phys.*, 1991, **94**, 831.
9 M. A. Vincent, J. N. L. Connor, M. S. Gordon and G. C. Schatz, *Chem. Phys. Lett.*, 1993, **203**, 415.
10 N. O. J. Malcolm and J. J. W. McDouall, *J. Phys. Chem.*, 1994, **98**, 12 579.
11 Y. Bu, Z. Cao and X. Song, *Int. J. Quantum Chem.*, 1996, **57**, 95.
12 B. C. Garrett, D. G. Truhlar, A. F. Wagner and T. H. Dunning Jr., *J. Chem. Phys.*, 1983, **78**, 4400.
13 G. C. Schatz, B. Amaee and J. N. L. Connor, *J. Phys. Chem.*, 1988, **92**, 3190.
14 M. González, J. Hijazo, J. J. Novoa and R. Sayós, *J. Chem. Phys.*, 1998, **108**, 3168.
15 A. Persky and H. Kornweitz, *J. Phys. Chem.*, 1987, **91**, 5496.
16 I. Last and M. Baer, *J. Chem. Phys.*, 1984, **80**, 3246.
17 I. Last and M. Baer, *Int. J. Quantum Chem.*, 1986, **29**, 1067.
18 D. K. Bondi, J. N. L. Connor, J. Manz and J. Römelt, *Mol. Phys.*, 1983, **50**, 467.
19 MOLPRO is a package of *ab initio* programs written by H-J. Werner and P. J. Knowles, with contributions from R. D. Amos, A. Berning, D. L. Cooper, M. J. O. Deegan, A. J. Dobbyn, F. Eckert, C. Hampel, T. Leininger, R. Lindh, A. W. Lloyd, S. J. McNicholas, W. Meyer, M. E. Mura, A. Nicklass, P. Palmieri, K. Peterson, R. Pitzer, P. Pulay, G. Rauhut, M. Schütz, H. Stoll, A. J. Stone and T. Thorsteinsson.
20 G. D. Purvis III and R. J. Bartlett, *J. Chem. Phys.*, 1982, **76**, 1910.
21 P. J. Knowles, C. Hampel and H.-J. Werner, *J. Chem. Phys.*, 1993, **99**, 5219.
22 R. J. Bartlett, *J. Phys. Chem.*, 1989, **93**, 1697.
23 M. Urban, J. Noga, S. J. Cole and R. J. Bartlett, *J. Chem. Phys.*, 1985, **83**, 4041.
24 K. Raghavachari, G. W. Trucks, J. A. Pople and M. Head-Gordon, *Chem. Phys. Lett.*, 1989, **157**, 479.
25 J. D. Watts, J. Gauss and R. J. Bartlett, *J. Chem. Phys.*, 1993, **98**, 8718.
26 M. J. O. Deegan and P. J. Knowles, *Chem. Phys. Lett.*, 1994, **227**, 321.
27 H-J. Werner and P. J. Knowles, *J. Chem. Phys.*, 1985, **82**, 5053.
28 P. J. Knowles and H-J. Werner, *Chem. Phys. Lett.*, 1985, **115**, 259.
29 H-J. Werner, *Mol. Phys.*, 1996, **89**, 645.
30 H-J. Werner and P. J. Knowles, *J. Chem. Phys.*, 1988, **89**, 5803.
31 P. J. Knowles and H-J. Werner, *Chem. Phys. Lett.*, 1988, **145**, 514.
32 T. H. Dunning Jr., *J. Chem. Phys.*, 1989, **90**, 1007.
33 R. A. Kendall, T. H. Dunning Jr. and R. J. Harrison, *J. Chem. Phys.*, 1992, **96**, 6796.
34 S. F. Boys and F. Bernardi, *Mol. Phys.*, 1970, **19**, 553.
35 N. A. Besley, PhD Thesis, The University of Birmingham, 1997.
36 M. Baer, *Chem. Phys. Lett.*, 1975, **35**, 112.
37 M. Baer, *Chem. Phys.*, 1976, **15**, 49.
38 M. Baer, *Mol. Phys.*, 1980, **40**, 1011.
39 A. Marcías and A. Riera, *J. Phys. B*, 1978, **11**, L489.
40 H-J. Werner and W. Meyer, *J. Chem. Phys.*, 1981, **74**, 5802.
41 C. Petrongolo, G. Hirsch and R. J. Buenker, *Mol. Phys.*, 1990, **70**, 825.
42 G. Hirsch, R. J. Buenker and C. Petrongolo, *Mol. Phys.*, 1990, **70**, 835.
43 M. Peric, R. J. Buenker and S. D. Peyerimhoff, *Mol. Phys.*, 1990, **71**, 673.
44 A. J. Dobbyn and P. J. Knowles, *Mol. Phys.*, 1997, **91**, 1107.
45 F. Rebentrost and W. A. Lester Jr., *J. Chem. Phys.*, 1975, **63**, 3737.
46 F. Rebentrost and W. A. Lester Jr., *J. Chem. Phys.*, 1976, **64**, 3879.
47 F. Rebentrost and W. A. Lester Jr., *J. Chem. Phys.*, 1977, **67**, 3367.
48 F. T. Wall and R. N. Porter, *J. Chem. Phys.*, 1962, **36**, 3256.
49 A. F. Wagner, G. C. Schatz and J. M. Bowman, *J. Chem. Phys.*, 1981, **74**, 4960.
50 S. K. Gray, J. S. Wright and X. Chapuisat, *Chem. Phys. Lett.*, 1977, **48**, 155.
51 J. S. Wright and S. K. Gray, *J. Chem. Phys.*, 1978, **69**, 67.
52 J. N. L. Connor, *Comp. Phys. Commun.*, 1979, **17**, 117.
53 L. Visscher and K. G. Dyall, *Chem. Phys. Lett.*, 1995, **239**, 181.

Paper 8/08183B